UDC 539.4

Stacking Sequence Effect on the Fracture Behavior of Narrow L-Shaped Cross-Ply Laminates: Experimental Study

Z. Y. Pan,[a,b] Q. F. Duan,[c] Y. C. Zhong,[c] S. X. Li,[a] and D. F. Cao[a,1]

[a] State Key Laboratory of Materials Synthesis and Processing, Wuhan University of Technology, Wuhan, China

[b] Department of Civil and Structural College, Wuhan Huaxia University of Technology, Wuhan, China

[c] School of Science, Wuhan University of Technology, Wuhan, China

[1] Caodongf@163.com

The stacking sequence effect of narrow L-shaped laminates on the fracture mode was studied. Two laminate stacking sequences were designed to analyze different fracture modes. The sequence layup J, i.e., $[0/90_4/0_2/90_2/0_2/90_2/0_2/90]_s$ trends to highlight the matrix fracture mode, whereas the stacking sequence layup I, i.e., $[0_4/90/0_3/90/0_2/90_2/0_2/90]_s$ tends to highlight the delamination mode. Load–deflection curves and fracture modes for these stacking sequences under a four-point bending loads were recorded and compared with the plane-strain empirical formula and experimental results. The results show that the stacking sequence has a significant effect on the initial fracture mode of narrow L-shaped laminar composites. Layup J shows matrix-dominant initial fracture due to the weak resistance of inner 90° plies to tangential tensile stresses, whereas layup I experiences delamination-dominant initial failure. The edge effect has a great influence on the fracture mode of layup J-like specimens, whereas it is very weak for layup I-like ones. The stacking sequence also influences the carrying capacity; a maximum fracture load of layup J is apparently lower than that of layup I, by about 23%.

Keywords: stacking sequence, L-shaped, fracture mode, matrix cracking, composites.

Introduction. Advances in the composite-related technologies with a high demand of light-weight structures imply a wide usage of composite laminates in the primary load-carrying components [1]. In particular, L-shaped composite laminates are widely used in wind energy industries, aerospace, etc. In general, L-shaped structural components made from unidirectional (UD) composites exhibit a relatively single delamination-dominant fracture mode. The weak resistance of laminates to opening radial stresses (positive radial normal) is extremely apt to cause interlaminar debonding. However, for an L-shaped laminate with multidirectional plies, a unique three-dimensional behavior with complicated progression of matrix cracking and fibre failure [2] also appears in addition to the well-known interlaminar delamination. Under an unfolding bending load, the inner plies of L-shaped laminates bear high tangential tensile stresses, which cause radial (or transverse) matrix cracks to develop in the off-axis plies due to poor resistance of matrix to tangential tensile stresses. If a radial crack occurs, singular stresses may also induce a local delamination where the matrix crack reaches the adjacent plies. For narrow specimens of multidirectional plies, bending loads lead to singular stresses at the free edges of specimens, due to the difference in material properties between adjacent plies with different orientations. This edge effect may significantly reduce the failure loads, which are substantially below that predicted by 2D, plane strain analysis. In addition, earlier mentioned fracture modes may interact with each other and further increase the complexity of the crack onset and propagation in L-shaped composite laminates. All the complex fracture modes are apparently dependent on stacking sequences. The stacking sequence

effect is important and can be tailored to influence tangential stresses in inner plies and singular stresses near free edges. Although the research on L-shaped laminates has attracted much attention [3–10], those related to the stacking sequence effect on the mechanical behavior of L-shaped laminates are quite scarce.

Sun and Kelly [11] performed a set of experimental studies where L-shaped composite structures of three different stacking sequences was investigated in detail. The experimental data and observations showed that the L-shaped laminate had two distinct fracture modes: transverse matrix cracking due to bending stress, and interlaminar delamination due to the high interlaminar normal stress in the direction of thickness. When initial crack was intralaminar matrix cracking, the structure still retained its load-carrying capacity after initial intralaminar matrix cracking. Another interesting study was carried out by Feih and Shercliff [12] who investigated the single-L peel joint made from multidirectional plies under bending deformation. Results showed that all specimens exhibited the delamination-dominated fracture mode. However, the first failure was matrix cracking under tension at the top 45° ply rather than delamination. Although above experimental data revealed the competition relationship of delamination and matrix cracking for initial cracks, the free edge effect was deliberately avoided by using very wide curved specimens. Wisnom [13] evaluated the effect of specimen width on edge effect in comparison with plane strain analysis. It was found that the edge effect was considered as negligible for wide curved specimens, i.e., the ratio of width to thickness is larger than 10. Although the final products in application may be very wide and/or may be incorporated into surrounding structure at their ends, large composite parts are typically certified by testing narrow specimens which have exposed free edges. Thus, it is interesting to understand the internal damage mechanisms, critical fracture modes and their effects on load-carrying capability of narrow L-shaped laminated composites. In this study, experimental studies on the stacking sequence effect on the fracture mode of narrow L-shaped laminates under the four-point bending is performed. Two laminate stacking sequences with the intention of isolating different modes of failure are designed. A four-point bending fixture (ASTM Standard D6415/D6415M [14]) has been employed to provide a pure bending moment. The load-displacement curves are recorded and fracture mode of cured region is dynamically detected and photographed. A comparative analysis with the plane-strain empirical formula has been carried out to evaluate the effect of stacking sequence on failure behavior of narrow L-shaped laminates.

1. Experimental Detail.

1.1. Test Specimen Preparation. The design of the L-shaped laminates is shown in Fig. 1. HTS40/977-2 prepreg material systems are used for the fabrication of test specimens. Two different layups specified are considered. The stacking sequence layup J, i.e., $[0/90_4/0_2/90_2/0_2/90_2/0_2/90]_s$ trends to highlight the matrix fracture mode, whereas the stacking sequence layup I, i.e., $[0_4/90/0_3/90/0_2/90_2/0_2/90]_s$ trends to highlight the delamination mode. The number of plies is 32 and the total thickness is 5.8 mm. Specimens are prepared using hand layup procedures and autoclave curing. The prepreg was cut into individual 0° and 90° plies (see direction definition shown in Fig. 1) measuring 200×200 mm. These were laid up over an angled positive mould made of invar steel, thus forming the 6.4 mm inner radius bend. The layup was covered by a 15 mm thick silicone pad, then sealed in a vacuum bag. The entire assembly was placed in an autoclave for curing.

Once cured, the completed L-shaped panel has been cut into individual test specimens with the width of in 25 mm using a diamond cutter. The machined edges of the specimens are kept flat and parallel, satisfying the ASTM Standard D6415/D6415M [14]. The designed geometry of L-shaped specimen is shown in Fig. 2. Following the cutting operation, the machined edges of the specimens were polished to provide smooth surfaces to aid visually detecting cracks during testing. The final specimens of layup I are exhibited in Fig. 2b.

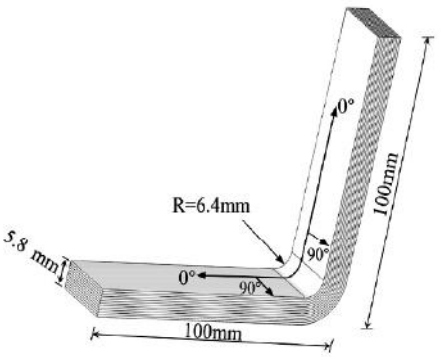

Fig. 1

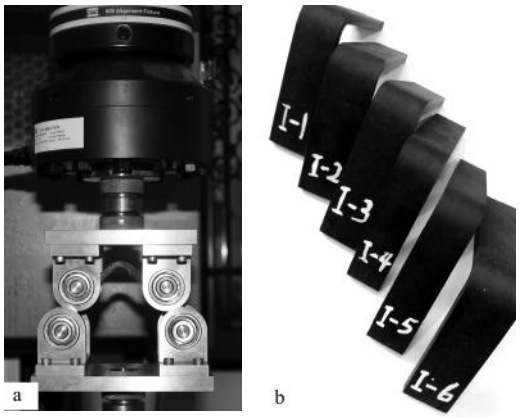

Fig. 2

Fig. 1. Schematic of L-shaped laminates.
Fig. 2. Four-point-bending fixture and specimens: (a) fixture; (b) specimens of layup I.

1.2. Experimental Setup and Procedures. A four-point-bending test fixture (Wyoming test Fixture Inc.) as shown in Fig. 2a is used to load the specimen. The cylindrical loading bars have diameters D of 10 mm and are mounted on roller bearings. An electro-hydraulic universal machine is used for the four-point bending tests. A displacement rate of 0.5 mm/min is applied during the tests.

The load and displacement outputs are recorded on the X–Y plotter, producing a load vs. displacement curve. A camera with macro lens was used to view the edges of the specimen in the curved region during each test. The load is applied under manual displacement control to permit careful scrutiny of the specimen during loading. The onset of damage and damage evolution could be dynamically detected and photographed.

2. Results and Discussion.

2.1. fracture mode Observation and Discussion. Figure 3 shows crack initiation and propagation in curved region for layups J and I.

All specimens of layup J exhibited matrix-dominated initial cracks in the innermost 90° plies. Subsequently, these matrix cracks continued to propagate and transformed into interlaminar cracks as the matrix cracks reached the adjacent 0° plies, shown in Fig. 3a. The matrix cracking is due to the large tangential tensile stresses and the weak resistance of 90° plies near the inner surface to tangential tensile stresses. As the bending loads increased, the second typical cracks occurred at the interface between the 9th and 10th ply, approximately at 29% of the thickness from the inner radius. At this point, layup J exhibited delamination-dominated cracks, followed by the crack kinking (the crack kinking refers to the cross-layer delamination defined by Wimmer et al. [15]), shown in Fig. 3b. This delamination, starting from the interlaminar delamination, grows across the 90° ply and then grows along the opponent interface. In the course of continued loading before gross failure occurred, the failure presents the same mode, i.e., delamination with the crack kinking (Fig. 3c).

In contrast, layup I specimens exhibited no initial matrix cracking, and failed in the delamination mode, as shown in Fig. 3d. The location of initial delamination occurred at 37.5% of the thickness from the inner radius. During the subsequent loading, the dominant fracture mode was still delamination-dominant failure, as shown in Fig. 3d–f. In addition, some crack kinking phenomenon accompanied by interlaminar delamination can be observed, when the delamination propagated along the certain interface between 0° and 90° plies.

Next, the test results will be compared with the wide-specimen experimental results of Sun et al. [11] and the plane-stain empirical formula of Lekhnitskii [14, 16].

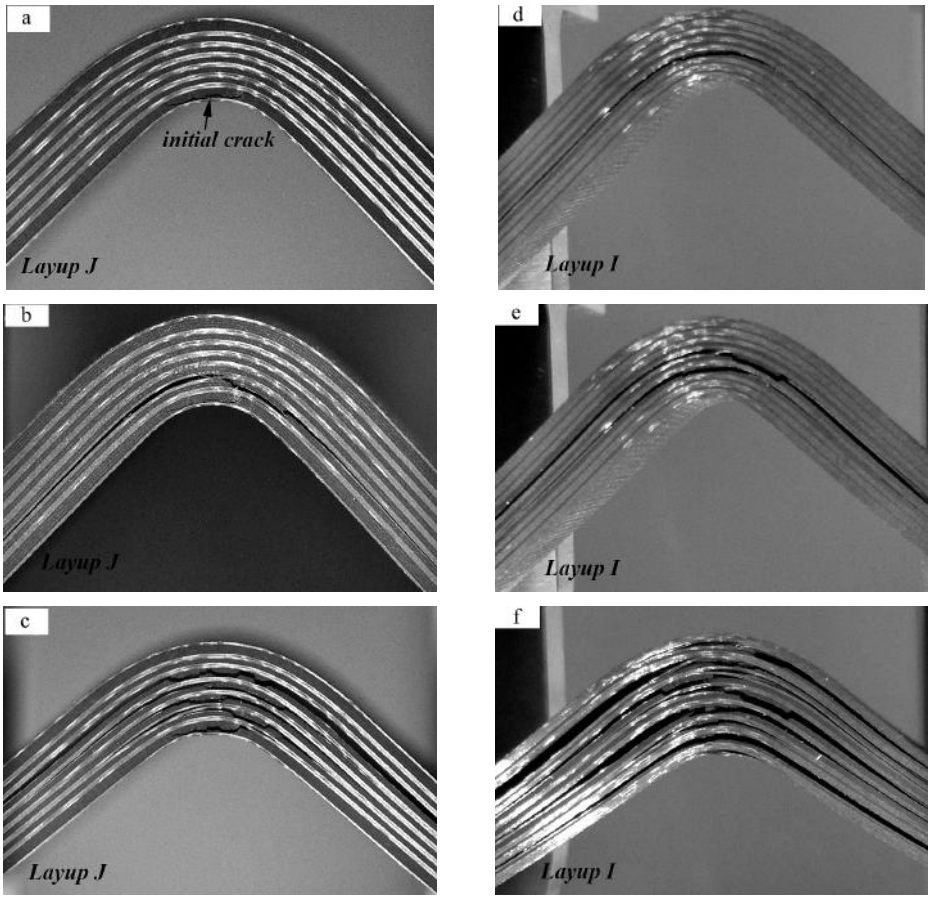

Fig. 3. Crack initiation and propagation in curved region for two deferent layups: (a–c) for layup J; (d–f) for layup I.

The specimens of this test have very similar stacking sequences with Sun et al.'s experiments and the major difference reflects in the ratio of width to thickness. The ratio of width to thickness in [11] was equal to 10 , while the edge effect was neglected, according to Wisnom's study [13]. In this study, the above ratio was 4.3, while a certain edge effect on fracture mode was observed. The initial failure, which was termed as radial cracking by Sun and Kelly [11, 17], also occurred in the inner 90° plies. However, in [11], initial cracks did not transform into interlaminar ones, which is not consistent with the current experimental observation. That means that the edge effect of narrow specimens on the evolution of initial matrix cracks for layup J was quite strong.

The fracture mode of layup I was almost the same with the corresponding experimental observation of [11](i.e., both specimens exhibited no initial matrix cracking, and failed directly in the delamination mode). Also, the location of initial delamination was consistent with [11], as well as the plane-strain empirical formula of Lekhnitskii [14, 16].

The radial position r_m of the maximum interlaminar (radial) tensile stress in a curved beam is given by Eq. (1) according to ASTM Standard D6415/D6415M [14]:

$$r_m = \left[\frac{(1-\rho^{\kappa-1})(\kappa+1)(\rho r_0)^{\kappa+1}}{(1-\rho^{\kappa+1})(\kappa-1) r_0^{1-\kappa}} \right]^{1/2\kappa}, \qquad (1)$$

where

$$g=\frac{1-\rho^2}{2}-\frac{\kappa}{\kappa+1}\frac{(1-\rho^{\kappa+1})^2}{1-\rho^{2\kappa}}+\frac{\kappa\rho^2}{\kappa-1}\frac{(1-\rho^{\kappa-1})^2}{1-\rho^{2\kappa}},\quad \rho=\frac{r_i}{r_o},\quad \kappa=\sqrt{E_\theta/E_r},$$

r_i and r_o are inner radius and outer radius of the specimen. The elastic moduli in the radial and tangential directions (E_r and E_θ) can be approximated by the classical and laminated shell theories, respectively. For layup I made from HTS40/977-2, $E_r = 11.3$ GPa, $E_\theta = 109.1$ GPa, $r_i = 6.4$ mm, and $r_o = 12.2$ mm are substituted in Eq. (1), $r_m = 8.55$ mm can be obtained. The initial delamination occurred at 36.9% of the thickness from the inner radius, which is mostly identical to our experimental observation. That means the edge effect is also negligible for a narrow specimen if a special stacking sequence is designed.

2.2. Load–Displacement Curves. As the experiments on the L-shaped laminates are conducted, load–displacement behavior is recorded. Figure 4 presents the moment–displacement curves of two layups, plotted as M, the moment per unit specimen width on the vertical axis and loading bars' displacement Δ on the horizontal axis. Following the ASTM Standard D6415/D6415M [14], M of curved laminate specimens is generated by 4 rollers, as shown schematically in Fig. 5 and calculated according to

$$M = P/(2w\cos\phi)\times[dx/\cos\phi+(D+t)\tan\phi], \tag{2}$$

$$\sin\phi=[-dx(D+t)+dx\sqrt{d_x^2+d_y^2-D^2-2Dt-t^2}]\Big/(d_x^2+d_y^2), \tag{3}$$

where P is the total force applied to the four-point-bending fixture, D is the diameter of the cylindrical loading bars on the four-point-bending fixture, t is the average thickness of specimen, and dx and dy are horizontal and vertical distances between two adjacent top and bottom loading bars, respectively.

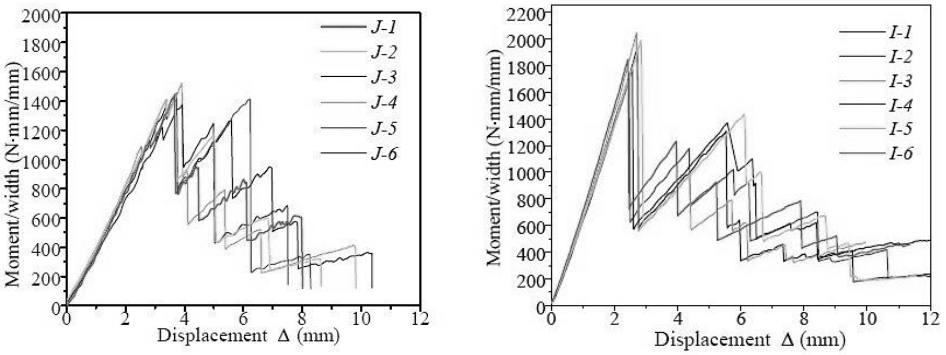

Fig. 4. Moment–displacement curves for layups J (a) and I (b).

For layup J, the specimens were loaded elastically until a small load drop at 2.8–3.4 mm of displacement Δ, as shown in Fig. 4a. The initial failure occurred with a breaking sound associated with an instantaneous delamination induced by matrix cracking (Fig. 3a). Linearly increasing load declined by 2.6–6.8% of the maximum failure load. In general, matrix cracking does not yield to failure of the specimen, but also, does not affect the load–displacement behavior [6]. However, in current structure design of L-shaped laminates, the matrix cracking instantaneously triggered the delamination which is the direct reason for small load drop. The load-carrying capability of the L-shaped specimen was recovered

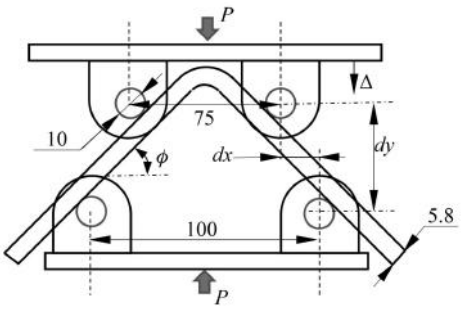

Fig. 5. Schematic of four-point curved beam setup [14] (unit: mm).

and continued to increase linearly until next load drop, following a small load drop. This load drop is directly due to the delamination, which occurs instantaneously with a loud sound of "bang" in parallel to the abrupt load drop in the load–displacement curves. After reaching the maximum value, the load dropped down to 53–67% of the maximum load. Meanwhile, a crack kinking across 90° plies happened at the same displacement, however, none of the crack kinking was visible from the load–displacement. In the course of continued loading, the load-displacement curve presented a ladder-shaped feature with delamination-dominant fracture mode before the gross failure occurred.

The load of layup I had not a small load drop, but always increased linearly until the maximum load occurred unlikely the load–displacement of layup J, as shown in Fig. 4b. This is due to the fact that layup I specimens did not exhibit any initial matrix cracking, and failed directly in the delamination mode. This delamination made the load drop down to 29–35%. The displacement Δ at the maximum failure load for layup I is about 2.5 mm, larger than that of layup J, about 3.5 mm. It is attributed to the higher module of layup I containing more 0° plies.

Failure loads for two layups of L-shaped specimens are summarized in Table 1, where "initial" refers to the load corresponding to the first failure, and "maximum" represents the peak load during the whole loading. It is noted that the maximum and initial failure loads are the same for layup I. From Table 1, the average maximum failure load of layup J is obviously lower than that for layup I. This result is not consistent with [11], where the maximum failure loads of both layups were almost identical. Our contrastive test has very similar stacking sequences to [11], with the major difference being in the width-to thickness ratio. In [11], very wide specimens with the ratio of 10 were used, so that plane-strain conditions could be assumed, whereas in our test the maximum failure load was reduced by the free edge effect, which is more pronounced in narrow test specimens (with the ratio of 4.3.

Next, the failure loads have to be evaluated, by comparing the maximum failure load with CBS based on the plane strain analysis. CBS is defined as the applied bending moment per unit width at failure and corresponds to the maximum failure load in the test. According to the ASTM Standard D6415/D6415M [14], an approximate calculation via Eq. (4), has been developed for CBS:

$$CBS = \sigma_r^{\max} r_0^2 g \left[1 - \frac{1-\rho^{\kappa+1}}{1-\rho^{2\kappa}} \left(\frac{r_m}{r_0} \right) - \frac{1-\rho^{\kappa-1}}{1-\rho^{2\kappa}} \rho^{\kappa+1} \left(\frac{r_0}{r_m} \right)^{\kappa+1} \right]^{-1} = 2112 \text{ N} \cdot \text{mm/mm}, \quad (4)$$

where I-mode interlaminar strength $\sigma_r^{\max} = 62.3$ MPa for HTS40/977-2 [9] is substituted in Eq. (4). A CBS based on the plane-strain assumption for the preset geometriy and material system can be obtained as 2112 N · mm/mm. For layups I and J, average CBSs are

T a b l e 1

Failure Loads for Two Layups of L-Shaped Specimens

Specimen	Layup J failure load (N·mm/mm)		Layup I failure load (N·mm/mm)	
	Initial	Maximum	Initial	Maximum
1	1125	1444	1929	1929
2	1391	1394	1709	1709
3	1220	1376	2045	2045
4	1400	1523	1785	1785
5	1223	1442	2045	2045
6	1358	1415	1827	1827
Average	1286	1432	1890	1890

1890 and 1432 N·mm/mm, respectively. The CBS values of layup I and J are lower by than those of the plane-strain case by 10 and 33%, respectively. That implies a strong stacking sequence effect on the CBS of multidirectional L-shaped laminates containing more 90° plies near the inner surface. Authors [17] reported that the critical delamination fracture mode occurred regardless of stacking sequence. Since the radial stresses depended predominantly on cross-sectional geometry, they could not be reduced by varying the stacking sequence [17]. But this conclusion only applies to the special case that the specimen has enough width so that a plane-strain condition can be met. For the narrow specimens of layup J used in this study, the free edge effect in conjunction with groups of 90° plies near the inner surface induces the transformation of initial matrix cracks into interlaminar ones, where the matrix cracks reached the adjacent 0° plies. Although this interlaminar crack caused a small drop (2.6–6.8% of the maximum failure load) in the load-displacement curve, it continued to influence the subsequent fracture mode and load-carrying capability of L-shaped components. The above analysis shows that the carrying capacity of layup J-like specimens is controlled by the edge effect, which effect is feeble in layup I-like specimens. This implies the edge effect can be reduced by optimizing the stacking sequence.

Conclusions. The stacking sequence effect on fracture modes of narrow L-shaped laminates was studied. Specimens with two different laminate stacking sequences were loaded quasi-statically under four-point-bending loading conditions. The relevant fracture modes and load–displacement curves were analyzed and compared with test results [11, 17] on wide specimens and the plane-strain empirical formula of Lekhnitskii [14, 16].

Given this, the following conclusions are drawn:

1. The stacking sequence effect on the initial fracture modes of narrow L-shaped laminates near the curved region is quite strong. Layup I experienced a delamination-dominant initial failure, whereas layup J exhibited matrix-dominant initial cracking due to weak resistance of inner 90° plies to tangential tensile stresses.

2. In contrast to findings [11, 17], layup J presented a distinct fracture pattern of the edge effect, whereas layup I experienced a very similar fracture mode. It is concluded that fracture modes of L-shaped laminates are controlled not only by the stacking sequence, but also by the specimen width-to-thickness ratio. The edge effect was strong for layup J-like specimens and quite feeble for layup I-like ones. This strongly suggests that designers can reduce the edge effect of narrow specimens by optimizing their stacking sequence.

3. The layup I has the almost same carrying capacity as L-shaped laminates with plane-strain conditions. In contrast to his, the edge effect for layup J was found to reduce the failure load of curved laminates by over 30%. In view of the fact that large curved laminated parts are typically certified by testing narrow specimens, the certification method based on narrow specimens is found to be too conservative for layup J-like specimens.

1. B. Gozluklu, I. Uyar, and D. Coker, "Intersonic delamination in curved thick composite laminates under quasi-static loading," *Mech. Mater.*, **80**, 163–182 (2015).
2. R. H. Martin and W. C. Jackson, *Damage Prediction in Cross-Plied Curved Composite Laminates*, Technical Report NASA-TM-104089 (1991).
3. C. Thurnherr, R. M. J. Groh, P. Ermanni, and P. M. Weaver, "Investigation of failure initiation in curved composite laminates using a higher-order beam model," *Compos. Struct.*, **168**, 143–152 (2017).
4. M. H. Hassan, A. R. Othman, and S. Kamaruddin, "A review on the manufacturing defects of complex-shaped laminate in aircraft composite structures," *Int. J. Adv. Manuf. Tech.*, **91**, 4081–4094 (2017).
5. M. H. Hassan and A. R. Othman, "Contribution of processing parameters on void content in the vacuum bagging configurations of L-shaped composite laminates," *Int. J. Adv. Manuf. Tech.*, **93**, 1333–1345 (2017).
6. F. Georgiades, "Nonlinear equations of motion of L-shaped beam structures," *Eur. J. Mech. - A/Solid.*, **65**, 91–122 (2017).
7. M. Fiorina, A. Seman, B. Castanie, et al., "Spring-in prediction for carbon/epoxy aerospace composite structure," *Compos. Struct.*, **168**, 739–745 (2017).
8. C. Bellini, L. Sorrentino, W. Polini, and A. Corrado, "Spring-in analysis of CFRP thin laminates: numerical and experimental results," *Compos. Struct.*, **173**, 17–24 (2017).
9. Y. Shi and C. Soutis, "Modelling transverse matrix cracking and splitting of cross-ply composite laminates under four point bending," *Theor. Appl. Fract. Mec.*, **83**, 73–81 (2016).
10. S. Jimenez and R. Duddu, "On the parametric sensitivity of cohesive zone models for high-cycle fatigue delamination of composites," *Int. J. Solids Struct.*, **82**, 111–124 (2016).
11. C. T. Sun and S. R. Kelly, "Failure in composite angle structures Part I: Initial failure," *J. Reinf. Plast. Comp.*, **7**, 220–232 (1988).
12. S. Feih and H. R. Shercliff, "Composite failure prediction of single-L joint structures under bending," *Compos. Part A - Appl. S.*, **36**, 381–395 (2005).
13. M. R. Wisnom, "3-D Finite Element Analysis of Curved Beams in Bending," *J. Compos. Mater.*, **30**, 1178–1190 (1996).
14. *ASTM D6415/D6415M. Standard Test Method for Measuring the Curved Beam Strength of a Fiber-Reinforced Polymer-Matrix Composite*, ASTM International, West Conshohocken, PA (2006).
15. G. Wimmer, W. Kitzmüller, G. Pinter, et al., "Computational and experimental investigation of delamination in L-shaped laminated composite components," Eng. Fract. Mech., 76, 2810–2820 (2009).
16. S. Lekhnitskii, *Theory of Elasticity of an Anisotropic Body* [in Russian], Mir, Moscow (1981).
17. C. T. Sun and S. R. Kelly, "Failure in composite angle structures Part II: Onset of delamination," *J. Reinf. Plast. Comp.*, **7**, 233–244 (1988).

Received 15. 09. 2017